REPORT DOCUMENTATION PAGE

Form Approved OMB NO. 0704-0188

1. REPORT DATE (DD-MM-YYYY)	2. REPORT TYPE	3. DATES COVERED (From - To)
18-03-2015	Final Report	1-Jun-2012 - 31-May-2013

4. TITLE AND SUBTITLE
Final Report: Advanced Thermal Conversion Systems

5a. CONTRACT NUMBER
W911NF-12-1-0134

5b. GRANT NUMBER

5c. PROGRAM ELEMENT NUMBER

6. AUTHORS
Nicholas A. Melosh

5d. PROJECT NUMBER

5e. TASK NUMBER

5f. WORK UNIT NUMBER

7. PERFORMING ORGANIZATION NAMES AND ADDRESSES
Stanford University
3160 Porter Drive
Suite 100
Palo Alto, CA 94304 -1212

8. PERFORMING ORGANIZATION REPORT NUMBER

9. SPONSORING/MONITORING AGENCY NAME(S) AND ADDRESS (ES)
U.S. Army Research Office
P.O. Box 12211
Research Triangle Park, NC 27709-2211

10. SPONSOR/MONITOR'S ACRONYM(S)
ARO

11. SPONSOR/MONITOR'S REPORT NUMBER(S)
62174-CH-DRP.1

12. DISTRIBUTION AVAILIBILITY STATEMENT
Approved for Public Release; Distribution Unlimited

13. SUPPLEMENTARY NOTES
The views, opinions and/or findings contained in this report are those of the author(s) and should not contrued as an official Department of the Army position, policy or decision, unless so designated by other documentation.

14. ABSTRACT
This project evaluated the scientific and technical feasibility of a solar energy converter based on photon enhanced thermionic emission (PETE), which enhances thermionic emission with light. In order to achieve this goal, we focused the work on two objectives: (1) demonstrating that a structurally stable solar-enhanced converters can be created using microfabrication techniques and (2) Identifying materials that could function primarily as PETE emitters rather than just thermionic materials. The first objective addressed the challenges of achieving sufficient thermal isolation, structural stability, and optimal cathode-anode separation. The second objective addressed the

15. SUBJECT TERMS
PETE process, Solar, thermal isolation, optimal cathode-anode separation

16. SECURITY CLASSIFICATION OF:			17. LIMITATION OF ABSTRACT	15. NUMBER OF PAGES	19a. NAME OF RESPONSIBLE PERSON
a. REPORT	b. ABSTRACT	c. THIS PAGE			Nicholas Melosh
UU	UU	UU	UU		19b. TELEPHONE NUMBER 650-724-3679

Report Title

Final Report: Advanced Thermal Conversion Systems

ABSTRACT

This project evaluated the scientific and technical feasibility of a solar energy converter based on photon enhanced thermionic emission (PETE), which enhances thermionic emission with light. In order to achieve this goal, we focused the work on two objectives: (1) demonstrating that a structurally stable solar-enhanced converters can be created using microfabrication techniques and (2) Identifying materials that could function primarily as PETE emitters rather than just thermionic materials. The first objective addressed the challenges of achieving sufficient thermal isolation, structural stability, and optimal cathode-anode separation. The second objective addressed the challenges of discovering the materials that can efficiently absorb sunlight and
transform the absorbed photon energy and heat into high-energy electrons that lie at the heart of a PETE converter.

Enter List of papers submitted or published that acknowledge ARO support from the start of the project to the date of this printing. List the papers, including journal references, in the following categories:

(a) Papers published in peer-reviewed journals (N/A for none)

Received Paper

TOTAL:

Number of Papers published in peer-reviewed journals:

(b) Papers published in non-peer-reviewed journals (N/A for none)

Received Paper

TOTAL:

Number of Papers published in non peer-reviewed journals:

(c) Presentations

Number of Presentations: 0.00

Non Peer-Reviewed Conference Proceeding publications (other than abstracts):

Received Paper

TOTAL:

Number of Non Peer-Reviewed Conference Proceeding publications (other than abstracts):

Peer-Reviewed Conference Proceeding publications (other than abstracts):

Received Paper

TOTAL:

Number of Peer-Reviewed Conference Proceeding publications (other than abstracts):

(d) Manuscripts

Received Paper

TOTAL:

Number of Manuscripts:

Books

Received Book

TOTAL:

Received Book Chapter

TOTAL:

Patents Submitted

Patents Awarded

Awards

Graduate Students

NAME	PERCENT_SUPPORTED

FTE Equivalent:
Total Number:

Names of Post Doctorates

NAME	PERCENT_SUPPORTED

FTE Equivalent:
Total Number:

Names of Faculty Supported

NAME	PERCENT_SUPPORTED

FTE Equivalent:
Total Number:

Names of Under Graduate students supported

NAME	PERCENT_SUPPORTED

FTE Equivalent:
Total Number:

Student Metrics

This section only applies to graduating undergraduates supported by this agreement in this reporting period

The number of undergraduates funded by this agreement who graduated during this period: .....

The number of undergraduates funded by this agreement who graduated during this period with a degree in science, mathematics, engineering, or technology fields:.....

The number of undergraduates funded by your agreement who graduated during this period and will continue to pursue a graduate or Ph.D. degree in science, mathematics, engineering, or technology fields:.....

Number of graduating undergraduates who achieved a 3.5 GPA to 4.0 (4.0 max scale):.....

Number of graduating undergraduates funded by a DoD funded Center of Excellence grant for Education, Research and Engineering:.....

The number of undergraduates funded by your agreement who graduated during this period and intend to work for the Department of Defense .....

The number of undergraduates funded by your agreement who graduated during this period and will receive scholarships or fellowships for further studies in science, mathematics, engineering or technology fields: .....

Names of Personnel receiving masters degrees

NAME

Total Number:

Names of personnel receiving PHDs

NAME

Total Number:

Names of other research staff

NAME	PERCENT_SUPPORTED

FTE Equivalent:
Total Number:

Sub Contractors (DD882)

Inventions (DD882)

Scientific Progress

See attached.

Technology Transfer

Defense Sciences Research & Technology
Defense Sciences Office (DSO)

Contract
DARPA W911NF-12-1-0134

"Photon-Enhanced Thermionic Energy Converters for Solid-State Solar-Thermal Generators"

Final Report

Stanford University
SPO # 49492

An Educational Entity

Principle Investigators:

Nicholas A. Melosh
Associate Professor, Materials Science and Engineering

Technical Contact:
Dr. Nicholas Melosh
McCullough 223
476 Lomita Mall
Stanford University, Stanford CA 94305
phone: (650) 724-3679
FAX: (650) 736-1984
e-mail: nmelosh@stanford.edu

Administrative Contact:
Ms. Karen Hurdle
340 Panama Street
Stanford University, Stanford CA 94305
phone: (650) 721-6394
e-mail: khurdle@stanford.edu

Executive Summary

This project evaluated the scientific and technical feasibility of a solar energy converter based on photon enhanced thermionic emission (PETE), which enhances thermionic emission with light. In order to achieve this goal, we focused the work on two objectives: (1) demonstrating that a structurally stable solar-enhanced converters can be created using microfabrication techniques and (2) Identifying materials that could function primarily as PETE emitters rather than just thermionic materials. The first objective addressed the challenges of achieving sufficient thermal isolation, structural stability, and optimal cathode-anode separation. The second objective addressed the challenges of discovering the materials that can efficiently absorb sunlight and transform the absorbed photon energy and heat into high-energy electrons that lie at the heart of a PETE converter.

Background

This proposal describes an aggressive project to demonstrate a breakthrough concept toward high-efficiency, solid-state solar-thermal energy conversion: photon-enhanced thermionic emission (PETE). In contrast to conventional thermionic converters, PETE makes use of the high per-quanta energy of the photons in combination with thermal energy, to increase electron emission from the cathode. A two-stage, PETE topping stage followed by a thermoelectric bottoming stage, is projected to have a conversion efficiency of >50% for a cathode temperature several hundred degrees lower than needed by a conventional thermionic topping stage. PETE converter fabrication leverages several nanofabrication and MEMS processing techniques, such as nano-texturing of the cathode for efficient photon absorption and electron emission, surface micromachining for low-thermal conductivity interconnections, wafer-bonded, sealed vacuum cavities, and through-substrate vias. An all-solid-state, solar-thermal generator would supply a scalable, modular new source of electric power in the sub-500-Watt range that would significantly reduce DoD fuel requirements, especially for remote, forward-operating bases. However, several fundamental challenges must be overcome before the technology is practical enough for deployment, which is the purpose of this program. Much of the results have been summarized and reported in two publications [1] and [2].

Photon-Enhanced Thermionic Emission (PETE) Concept

PETE converters differ from conventional thermionic converters in their harvesting of the large energy supplied by photon absorption in the semiconductor photocathode (electron emitter), as illustrated in the by the energy-band diagrams in Fig. 1. In that aspect, PETE converters are similar to photovoltaic (PV) cells, but unlike PV cells, PETE converters can also operate at elevated temperatures and use the heat produced by the absorbed light. As a result, PETE efficiencies can exceed those of both conventional thermionic converters and PV cells.

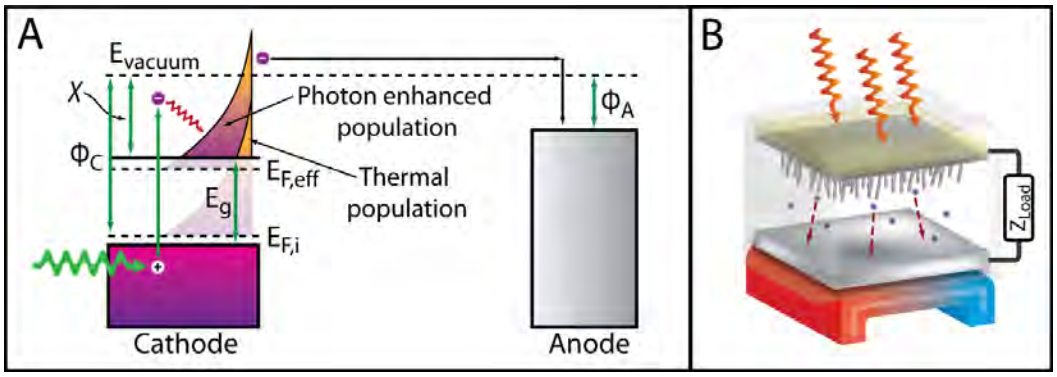

Figure 1. (a) Energy diagram of the PETE process. Photo-excitation leads to enhanced conduction band electron population, leading to larger thermionic currents and allowing the device to harvest both photon and heat energy. (b) Conceptual implementation of a parallel-plate PETE converter. Photons impinge on a nanostructured cathode and excite electrons, which then emit into vacuum and are collected by an anode. Unused heat from the PETE cycle is used to drive a bottoming cycle, shown schematically as a thermal engine.

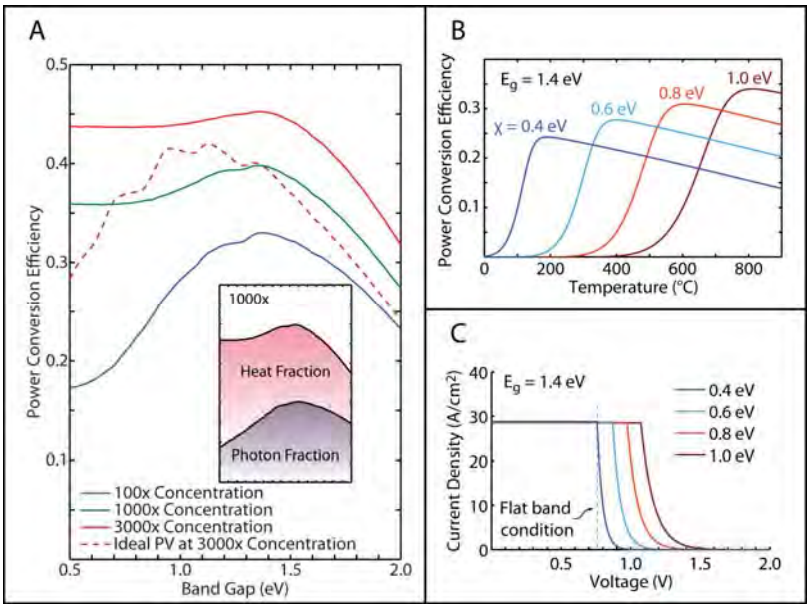

Figure 2. (a) PETE efficiency for the AM1.5 direct + circumsolar spectrum as a function of band gap. Cathode temperature and electron affinity are chosen to maximize overall efficiency. (Inset) The power output at 1000x is due to roughly equal contributions from thermal (χ) and photon (E_g) energy. (b) Power conversion efficiency at a concentration of 1000x increases with electron affinity χ due to larger voltage, but requires higher temperatures. (c) *J-V* curves for PETE devices with the same electron affinities in (b), with each operating at temperatures at which the efficiency is maximized.

The PETE process can be over 40% efficient at reasonable solar concentrations (1,000-3,000 suns) and temperatures (500-800ºC), as illustrated in Fig. 2(a). The major advantage of PETE over solar cells is that it uses both photon energy and thermal energy at the same time; thus, the "waste" heat from recombination losses or sub-bandgap light absorption is recycled. Therefore, PETE can surpass the Shockley-Queisser limit for single-junction photovoltaic cells at 3000x concentration (~38%). As shown in Fig. 2(b), the highest conversion efficiencies are obtained by using photo-cathodes with high electron affinities and correspondingly high operating

temperatures. The PETE diode's current-voltage curves for various electron affinities are shown in Fig. 2(c).

While the efficiency of a single PETE device can be higher than that of a PV device, the biggest advantage in efficiency comes from the fact that PETE operates at high enough temperatures that its waste heat can power a standard thermal conversion cycle, such as a thermoelectric converter (Fig. 3). The high operating temperatures of PETE makes it ideal as a topping stage, with the bottoming converter operating across a temperature difference of 250-350ºC to ambient.

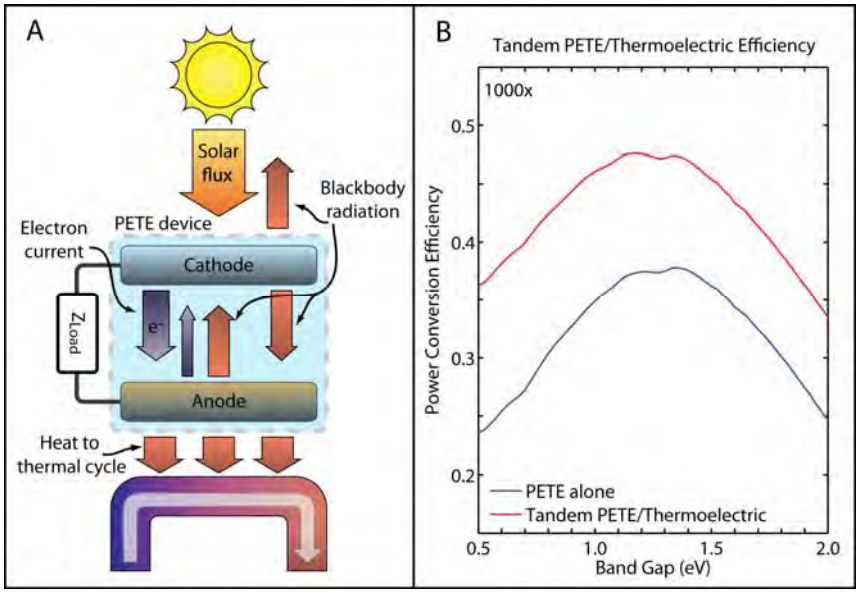

Figure 3. (a) Schematic of a PETE-thermal tandem energy converter. (b) Combined efficiency of the PETE-thermal tandem assuming a 20% efficiency of the bottoming thermoelectric stage [Melosh2009].

Objectives:

While these calculations are very favorable, creating materials and device architectures that can withstand the temperatures and cycling of both thermionic or PETE is a significant challenge. This program was aimed at demonstrating two main Objectives: (1) Creating and testing suspended , microfabricated electron emitters that can withstand the temperatures associated with thermionic emission and testing photon-enhancement, and (2) Identifying materials that could function primarily as PETE emitters rather than just thermionic materials. Fabricating PETE devices requires micro/nanofabrication processes will enable lower cost, higher production volume PETE converters. Since the device area itself is relatively small (4" to 6"-diameter disc), the chances of it getting damaged under field conditions are smaller than for a (non-concentrated) solar panel of equivalent power. The concentrators, on the other hand, could be extremely lightweight and expendable by using plastic. Due to the modular design of such converters, it is feasible to carry a number of units to the field. Should damage occur in the field, only the damaged part need be exchanged, improving overall robustness of the system.

Based on the research goals, we developed the two key program objectives:

Program Objectives

	Objective 1: MEMS platform for PETE	**Objective 2: Materials for PETE**
Phase 1 (12 months)	Fabricate suspended, high-temperature stable electron emitters using microfabrication technology	Identifying materials that could function primarily as PETE emitters rather than just thermionic materials.

Research Results:

Objective 1. MEMS Platform for PETE

To demonstrate the feasibility of PETE energy conversion, we microfabricated and tested a thermionic converter element and showed enhanced emission upon illumination, depicted in Fig. 4. With a physical structure similar to that of an IR-imager's micro-bolometer array, a complete converter would consist of a wafer-scale array of these microfabricated suspended elements, though this test only looked at smaller arrays. The folded suspension beams are designed to provide thermal isolation of the central pad from the substrate and to accommodate the thermal expansion of the central pad. They can also be used for optional resistive heating of the structure for testing purposes, allowing the temperature of the cathode surface to be controlled independently of the incident light intensity. The photocathode layer is contacted electrically using deposited metal bond pads shown in Fig. 4.

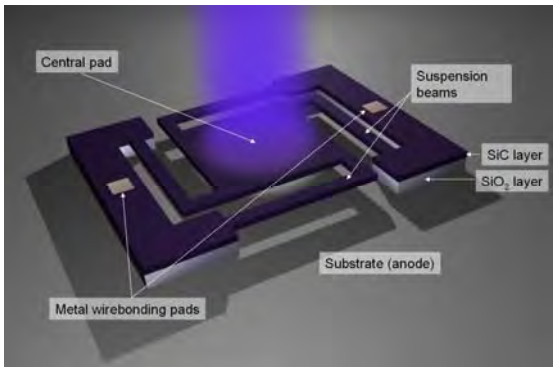

Fig. 4. Conceptual drawing of the thermionic and PETE demonstration microstructure.

Implementation

The emitter design consists of the center pad connected to the substrate by four bent "legs" as shown in Fig. 5. This design was selected to accommodate both the original film stress when the structure is being released and the large thermal expansion (of the order of 1%) that occurs at the typical operating temperatures of 1000–3000 K. The width of the legs was varied from 25 to 100 μm and the size of center pad from 500 to 900 μm. Etch holes were used in the central pad to facilitate the release of the structure.

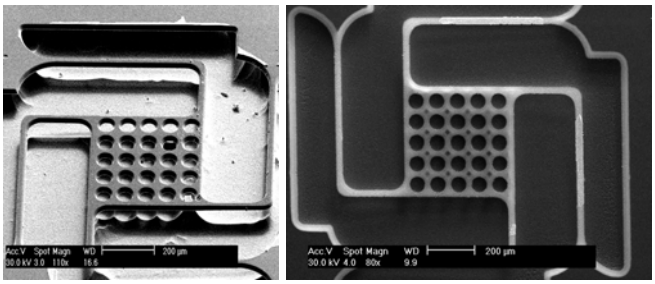

Figure 5: Scanning electron micrographs of microfabricated emitters made of single-crystal p-type 4H-SiC (left) and polycrystalline n-type 3C-SiC (right).

The fabrication process for p-type devices used bulk p-doped 4H-SiC wafers from CREE Inc. (360-μm thickness, ~1 Ohm·cm resistivity) and is shown in detail in Fig. 6. First, we cleaned a 1-cm-square die of SiC, as well as a silicon substrate with a 1.6 μm thick thermally grown oxide layer, in DI water, followed by a reverse RCA cleaning to remove any contamination and to obtain hydrophilic surfaces. The two substrates were then brought into contact and bonded together with approximately 10 MPa pressure applied at 450˚C. After lapping and polishing the 4H-SiC chip down to 50 μm thickness, it was blanket reactive ion etched down to approximately 10 μm thickness using mixed Cl_2, HBr, and O_2 plasma. A 4 μm thick low temperature oxide (LTO) hard mask was deposited and patterned using photolithography and BOE isotropic etching. The exposed silicon carbide layer was then anisotropically dry etched using the same RIE chemistry mentioned previously. Finally, the device was released using isotropic XeF_2 etching of the Si substrate followed by vapor HF etching of the SiO_2 layer.

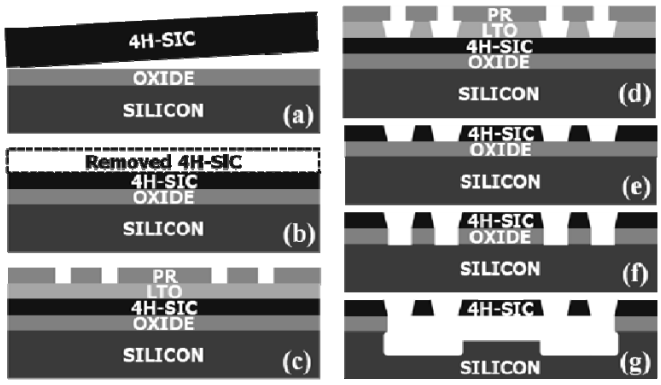

Figure 6: Outline of the fabrication process for p-type SiC emitters. The fabrication process for n-type devices followed steps (c) through (g) only.

In contrast to single crystal p-type emitters, the n-type emitters were fabricated out of a polycrystalline 3C-SiC thin film (2.6-μm thickness, ~0.03 Ohm·cm resistivity, 280 MPa tensile residual stress) deposited on SiO_2 sacrificial layer on silicon substrate. The rest of the fabrication process followed the same sequence of steps as for the p-doped devices (Fig. 6).

Experimental Development

After fabrication, the sample was mounted on an electrically isolated circuit board in a high-vacuum chamber (pressure < 10^{-5} Torr). One side (two legs) of the emitter was electrically grounded, and a negative voltage was applied to the other side (the other two legs) for resistive

heating. The collector (anode) of thermionic current was biased at +500V with respect to the ground to collect most (>80%) of the emitted electrons. In addition to Joule heating, the microfabricated emitters could be illuminated by focusing the output of an LED lightsource onto a ~1 mm diameter spot on the sample (Fig. 7). The field emission and pure photoemission currents were negligible for the emitter-anode distances, voltages, and wavelengths used.

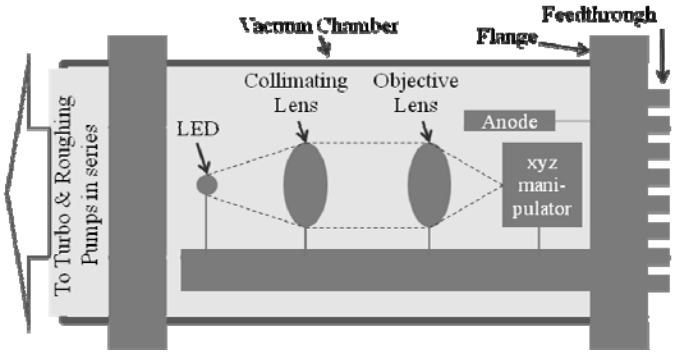

Figure 7: Diagram of optic setup mounted to vacuum chamber flange. (Show where the sample is in the setup as well, and perhaps the electrical connections)

N-Type 3C-SiC Emitters

To study thermionic emission properties, the microfabricated n-type emitters shown in Fig. 5 were heated resistively by passing DC current through them. Thermionic emission became detectable when the power dissipated in the device reached approximately 100 mW, and increased rapidly with the dissipated power, as shown by filled squares in Fig. 4. To study the effect of optical illumination and determine whether photon illumination enhanced emission, the light of a high-power LED with 455-nm center wavelength (2.8 eV photon energy) was focused on the device. The optically enhanced thermionic current was then measured and is shown by open triangles in Fig. 8. Since the incident photon energy is above the band gap of 3C-SiC (< 2.4 eV at elevated temperatures), some of the incident light was absorbed and produced photogenerated carriers. Consequently, the conductance of the emitter and Joule heating power varied by 1-2%. However, the larger effect was direct optical heating resulting from the thermalization and recombination of the photogenerated carriers. As a result, the illuminated curve is effectively shifted to the left of the dark curve by the amount of additional heating produced by the light. The shift varies from approximately zero at low DC heating powers to ~10 mW at high powers due to the temperature dependence of the band gap, which makes optical absorption stronger at higher temperatures.

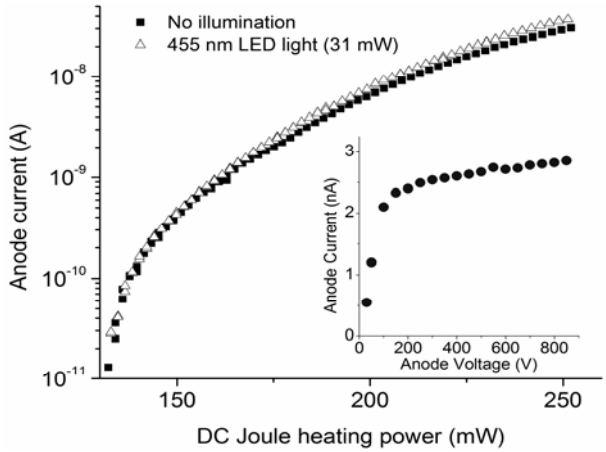

Figure 8: Effect of above-bandgap illumination on thermionic current from n-type 3C-SiC emitter. The inset shows the effect of the anode voltage on the collected current, indicating that the 500-V anode bias is sufficient to collect most of the emitted electrons.

For n-type devices, the main effect of optical illumination was limited to additional heating of the sample, as the number of photoexcited carriers was insignificant relative to the doped carrier population.

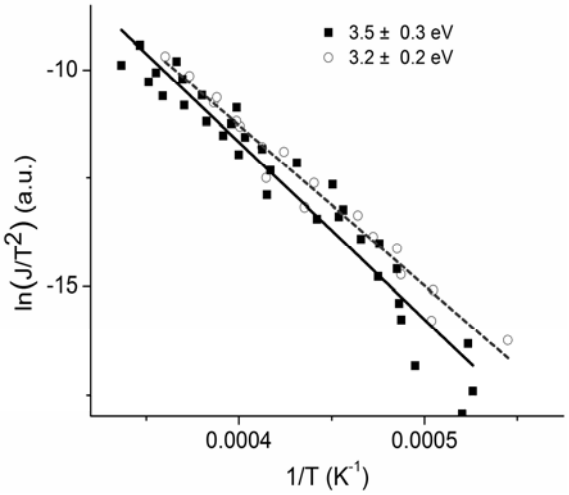

Figure 9: Richardson plot for two n-type 3C-SiC emitters.

At high temperatures (> 1000° C), the optical emissivity of 3C-SiC is sufficiently large to enable temperature measurements using an optical pyrometer (PYRO MicroTherm, 550-nm operating wavelength). This allowed us to fit the detected dark thermionic current (without optical illumination) to the Richardson-Dushman equation [3]: $J=A_E T_E^2 \exp(-\Phi_E/kT)$, where Φ_E is the emitter work function, T_E the emitter temperature, and A_E the materials-specific Richardson-Dushman constant. Figure 9 shows the resulting Richardson plots for two nominally identical microfabricated emitters. The work functions obtained from the fit were 3.5±0.3 eV and 3.2±0.2 eV, consistent with the work functions reported earlier for macroscopic 3C-SiC samples [5].

PETE Emitters based on p-type SiC

In p-type materials the additional conduction band carrier population created by photoexcitation can enable a new type of electron emission process. PETE combines photovoltaic and thermionic effects into a single physical process to take advantage of both the

high per-quanta energy of photons, and the available thermal energy due to thermalization and absorption losses [2]. The schematic of the PETE process is shown in Fig. 10 and consists of three steps. First, electrons in valence band are excited by photons into the conduction band. Second, they rapidly thermalize within the conduction band and diffuse throughout the emitter. Finally, electrons that reach the surface with energies greater than the electron affinity can emit into vacuum. The PETE process is advantageous compared to thermionic emission from n-type materials due to the larger output voltage, since the Fermi level is near the valence band rather than the conduction band.

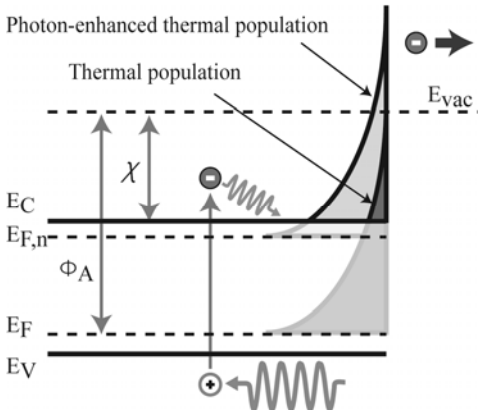

Figure 10: The PETE process. Photon generated electrons increases the conduction-band population, leading to effective work function decrement and enabling the device to harvest both photon and heat energy.

The PETE current can be found by calculating the conduction band population under illumination at elevated temperatures. The additional conduction band populations created by the light illumination are the same for both n- and p-type emitters if we assume that the absorption coefficient and the carrier lifetime are independent of dopant. However, the relative change in the conduction band population is much more dramatic in the p-type emitter compared to the n-type emitter. This leads to a large upward shift of the electron quasi-Fermi level in the p-type emitter and decrease in the effective work function. The PETE current can therefore be orders of magnitude larger than the dark thermionic current. However, a large PETE enhancement can be only observed up to certain temperature since eventually the intrinsic carriers dominate both the extrinsic carriers and the photon generated carriers, and the dark thermionic current becomes approximately equal to the PETE current.

Figure 11 shows the simulated PETE current from 4H-SiC emitter. For the simulation, we used the dimensions of our microfabricated device and the optical setup: the device size 500 μm^2, device thickness 10 μm and the focused spot size 500 μm^2. We also assumed the absorption coefficient of 100 cm^{-1}, the carrier life time of 0.2 μs, and no surface recombination. At high temperatures (>1600 K), there is no enhancement as intrinsic thermal carriers dominate, and the emission current is no longer determined by the number of photon-generated electrons. At intermediate temperatures (<1600 K), photogenerated carriers dominate, and thermionic emission depends on the incident light intensity. As the temperature is decreased further, fewer and fewer thermalized carriers in the conduction band overcome the electron affinity barrier, χ, and the PETE current becomes undetectably small.

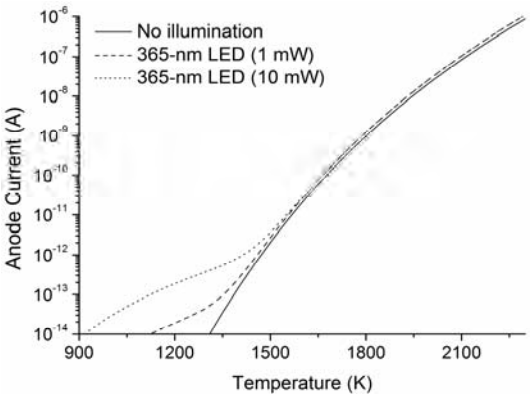

Figure 11: Simulation of PETE current from a p-type 4H-SiC emitter.

Experimentally, thermionic current from p-doped emitters became detectable when the power dissipated in the device reached approximately 50 mW as shown by filled squares in Fig. 12. Unexpectedly, thermionic emission decreased for DC heating powers in the range 150–230 mW. The nature of this "hump" is being investigated, but we believe it may be caused by temperature redistribution in the resistively heated device. Since thermionic current depends exponentially on the temperature of the emitter surface, it is largely determined by the temperature of the hottest part of the emitter. Although we expect the average temperature of the emitter to increase monotonically with dissipated power, the peak temperature could decrease because the resistivity and thermal conductivity of doped SiC depend strongly on the temperature.

To study the effect of optical illumination on the thermionic current, a high-power UV LED with 365-nm center wavelength (3.4 eV) was focused on the p-type 4H-SiC device. Since the incident photon energy is above the bandgap of 4H-SiC (< 3.2 eV at elevated temperatures), some of the incident light is absorbed and causes photon generated electrons in conduction band. The incident optical powers were estimated to be 0.48 mW, 2.57 mW, and 7.55 mW using an optical detector and a CCD camera.

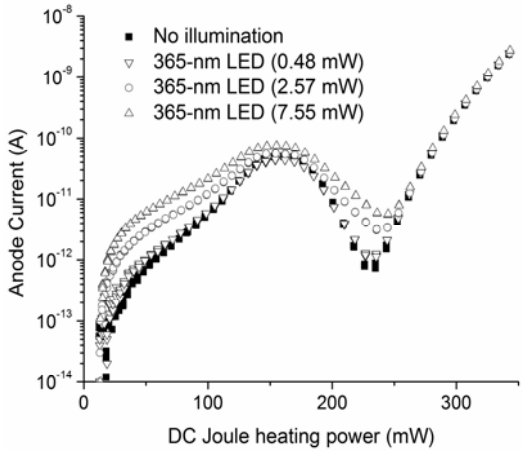

Figure 12: Experiment data of Photon Enhanced Thermionic Emission from p-type 4H-SiC emitter.

Figure 12 shows the experimental measurements of thermionic current versus resistive heating power both with and without illumination. For low heating powers (50–250 mW), the current is enhanced by about an order of magnitude due to the photon generated electrons. For

higher resistive heating powers (>250 mW), there is little change, as expected from the simulation above. For even higher Joule heating powers (not shown in Fig. 12), there is a noticeable increase in the thermionic current due to the effect of optical heating, just like in the case of n-doped emitters.

Figure 13 shows additional evidence that the observed current enhancement is in fact due to the PETE effect. According to the PETE model the electron concentration in the conduction band and therefore the PETE current depend linearly on the number of incident photons, consistent with Fig. 13. In contrast, optical heating would have resulted in approximately exponential dependence of the current on optical power.

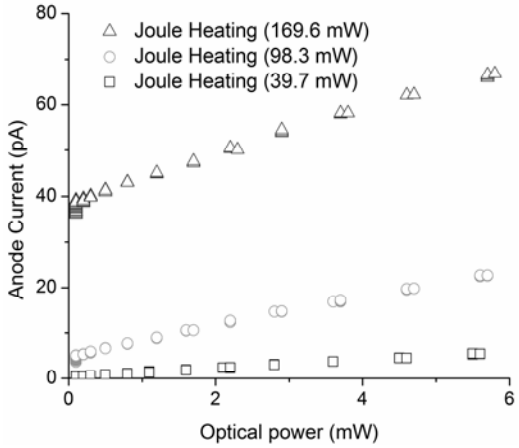

Figure 13: linearity dependence of Photon enhanced thermionic emission on incident light intensity.

This Objective was thus successful, and we were able to create microfabricated structures that were robust for thermionic emission, and also displayed improved characteristics upon illumination, demonstrating the PETE effect. We studied the effect of illumination on the thermionic current from thermally and mechanically robust microfabricated emitters with both n- and p-type doping. The p-type SiC emitter was used to demonstrate PETE in an uncesiated and microfabricated sample, bringing this energy conversion approach closer to practical applications.

Objective 2: Materials for PETE

In the PETE process, thermal energy is used to boost photo-excited electrons in the conduction band into vacuum. This process is analogous to thermionic emission, except that photo-excitation adds between 0.5–1.0 V to the operating voltage and reduces the required thermionic temperatures by 500–1000ºC. Ideal materials for PETE have indirect band-gaps in the 1.1–1.8 eV range, low recombination rates, and good thermal stability [2]. Materials such Si, Ge, InGaP, and GaN are thus interesting (though not necessarily ideal) candidates.

For task 2, we demonstrated the PETE emission process in cesiated GaN, where the emitted electrons have energy higher than possible with electrons alone, as reported in [2]. GaN samples were loaded into an ultra-high vacuum chamber (low 10^{-10} Torr base pressure) with sample heating, monochromatic illumination, and electron energy analysis capabilities. The GaN was carefully dosed with Cs vapor to lower the electron affinity to roughly 0.3-0.4eV, as determined by the low energy cutoff of emitted electrons. In Fig. 14a, the emitted electron energy

distributions with 3.75eV (330nm) illumination are shown as a function of temperature. The distributions have the characteristic shape of thermally emitted electrons, as the distribution widths broaden with temperature. The slight non-monotonic temperature dependence of the peak position is due to a ~25meV change in the sample's work function relative to that of the analyzer over the course of measurement, but this shift does not affect the broadening results.

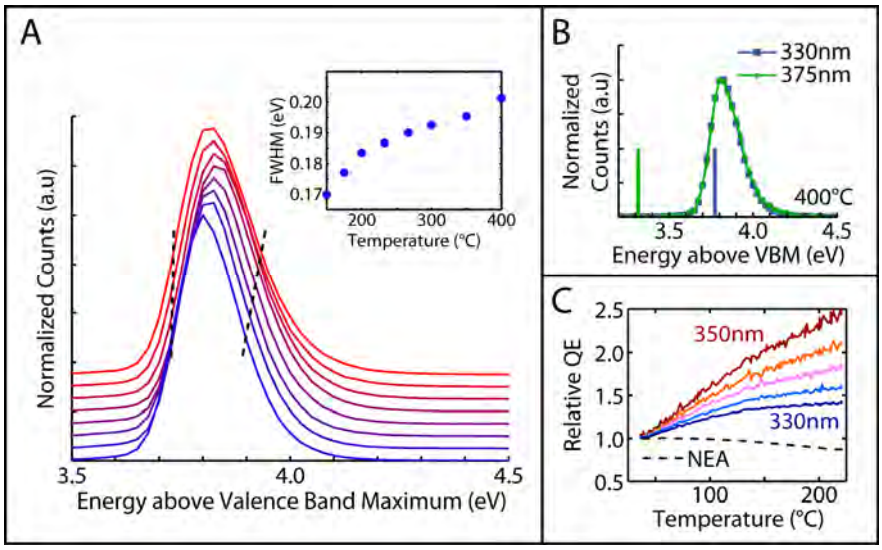

Figure 14: Temperature dependent measurements of [Cs]GaN. **a**, Energy distributions of electrons emitted from GaN at 330nm. The inset shows that the electron distribution's full width at half maximum (FWHM) increases with temperature. As noted in the Methods section, the temperature calibration in parts a and b are with respect to a silicon reference and are only approximate. **b**, Electron energy distributions at 400°C under 330nm and 375nm illumination. Measured photon energies are shown as vertical lines. These curves have been normalized to emphasize line shape, and emission current under 375nm illumination is substantially less since absorption at this wavelength is weaker. Purely thermionic emission from this sample in the absence of illumination is considerably smaller but occurs in the same energy range. **c**, Emission current of a sample with electron affinity close to the positive/negative crossover as a function of temperature for 3.5eV (350nm) illumination. The emission current of the same sample near-optimally cesiated to a state of negative electron affinity at 350nm illumination is shown as a black dashed line for reference. These traces have been normalized to emphasize temperature dependence. The temperature range is less than in parts a and b because the NEA coating does not survive to high temperature.

Fig. 14b provides further confirmation that at high temperatures the electrons thermalized before emission and provides a powerful example of the potential of PETE for power conversion. The sample was illuminated with either 3.75eV photons (330nm, energy approximately equal to the work function) or 3.3eV photons (375nm, energy barely exceeding the bandgap at 400ºC). The two distributions are virtually identical, indicating the electron energy distribution immediately following photoexcitation was unimportant, as would be expected from PETE. Interestingly, since the average emitted electron energy was approximately 3.8 eV, each electron excited with 3.3eV light acquired ~0.5eV in thermal energy prior to emission. In an energy converter this thermal boost could be harvested by using a proportionately higher operating voltage. For small bandgap semiconductors, such as Si (1.1eV) or GaAs (1.4eV), a similar thermal boost would represent a considerable increase over the bandgap energy. The energy distribution without illumination was considerably smaller and has been subtracted from these curves, demonstrating the emission is not purely thermionic.

While electron thermalization most clearly identifies the PETE process, the electron yield increased with temperature as well. The temperature dependent emission current from a GaN sample with a small positive electron affinity was measured in a separate vacuum chamber (Fig. 14c). As the sample temperature varied from approximately 50 to 225ºC, the emission current from 350nm illumination more than doubled. The increase in yield for higher energy photons was less dramatic, likely reflecting a contribution from direct photoemission which decreases with temperature due to increased scattering. For comparison, the same sample was further dosed with cesium to reach a state of negative electron affinity (NEA), with the result shown as a black dashed line in Fig. 14c. The stability of the NEA coating restricted the maximum temperature for these experiments to ~200ºC. Because electrons do not need to overcome an additional barrier at the surface when the electron affinity is highly negative, the dominant temperature effect at 350nm is a reduction in diffusion length. As a result, this trace shows a weak decrease in yield with temperature, clearly differentiating photoemission vs PETE processes.

While cesiated GaN was convenient for demonstrating photon enhancement of thermionic emission, efficient solar power conversion based on the PETE effect requires consideration of several factors in addition to thermal and chemical stability, most notably absorption and recombination. Only 1% of solar photons have energies exceeding GaN's 3.3 eV band gap, making the material unsuitable for solar applications. GaN's high defect density and surface recombination, along with sub-optimal absorption due to the sample's thin film geometry, resulted in low PETE efficiencies: at 330nm, the quantum efficiency was around 0.14%. One route to overcoming challenges relating to absorption and recombination is using nanostructures, which have displayed long minority carrier lifetimes due to high crystallinity and low defect densities as well as significantly enhanced absorption over thin films [6,7]

Thus while Objective 2 was successful in identifying a PETE material, for high efficiency applications other systems with smaller bandgaps but similar thermal stability and electron emission properties will be needed. This work has paved the initial path towards such devices, and has proven the concept of microfabricated thermionic emitters with photon enhancement as well as demonstrated higher electron energy from one possible PETE material.

References

[1] J.-H. Lee, I. Bargatin, J. Provine, F. Liu, M.-K. Seo, M.L. Brongersma, R. Maboudian, N.A. Melosh, Z.-X. Shen, R.T. Howe, *Effect of illumination on thermionic emission from microfabricated silicon carbide structures*, Technical Digest Transducers 2011 (Beijing, China, June 5-9, 2011)

[2] J.W. Schwede, I. Bargatin, D.C. Riley, B.E. Hardin, R.T. Howe, Z.-X. Shen, N.A. Melosh, *Photon enhanced thermionic emission for solar concentrator systems*, Nature Mater. 10, 762-767 (2010)

[3] Hatsopoulos G N, Gyftopoulos E P, "Thermionic Energy Conversion, Vol. 1", MIT Press, 1978.

[4] J.-H. Lee, I. Bargatin et al., "Thermionic emission from microfabricated silicon carbide filaments", *Technical Digest PowerMEMS2009 workshop, Washington, DC*, December 1-4, 2009, pp. 149-152.

[5] G.G. Gnesin, G.S. Oleinik, L.N. Okhremchuk, I.A. Podehernyaeva, V.S. Fomenko, "Work function of polycrystalline silicon carbide", High Temperature, Vol. 8, pp. 623-626, 1970.

[6] Guichard, A. R., Barsic, D. N., Sharma, S., Kamins, T. I. & Brongersma, M. L. Tunable light emission from quantum-confined excitons in TiSi2-catalyzed silicon nanowires. *Nano Letters* **6**, 2140-2144, doi:Doi 10.1021/Nl061287m (2006).

[7] Zhu, J. *et al.* Optical Absorption Enhancement in Amorphous Silicon Nanowire and Nanocone Arrays. *Nano Lett* **9**, 279-282, doi:Doi 10.1021/Nl802886y (2009).